Relevant Material for Lecture 8

"Galaxies: Structure, Dynamics, and Evolution"

4. Structure of Dark Matter halos

Obviously, we cannot observe the dark matter halos directly - but we can measure the total density profiles of clusters, and we can check in our simulations what we expect for dark matter halos.

4.1 Theory of halo collapse

We define a halo as a region in which the density is larger than 200 times the critical density ρ_{cr}. This definition serves well to describe the collapsed part of the halo.
Hence the mass M is given by

$$M = \frac{4\pi}{3} r_{200}^3 200 \rho_{cr}$$

Since the critical density is given by

$$\rho_{cr}(z) = \frac{3H^2(z)}{8\pi G}$$

we find

$$M = \frac{100 r_{200}^3 H^2(z)}{G}$$

Hence the halo mass and the size are uniquely related - and the relation changes as a function of redshift.
The virial velocity of the halo is the circular velocity at the virial radius

$$V_{200}^2 = \frac{GM}{r_{200}}$$

Hence the halo mass, virial radius, and virial velocity are related by

$$M = \frac{V_{200}^3}{10GH(z)}$$

$$r_{200} = \frac{V_{200}}{10H(z)}$$

The Hubble constant $H(z)$ increases with lookback time. Hence at higher redshift, the size of a halo of a given mass is smaller than the size of a halo with the same mass at low redshift. Halos are more compact and denser at high redshift, which is exactly what we expect, as the density of the universe is higher at high redshift (by $(1+z)^3$).
Simulations show that the density profiles of halos are well approximated by a Navarro Frenk White profile (1997):

$$\rho(r) = \frac{\rho_s}{(r/r_s)(1+r/r_s)^2}$$

where ρ_s and r_s are scaling parameters. Hence at very small radii ($r < r_s$), $\rho \propto r^{-1}$, and at large radii ($r > r_s$) $\rho \propto r^{-3}$. At r_s, the slope of the density profile bends over.
We define a concentration parameter c by $c = r_{200}/r_s$. It is easy to show that

$$\rho_s = \frac{200}{3} \rho_{cr}(z) \frac{c^3}{ln(1+c) - c/(1+c)}$$

Hence the profile of the halo is completely determined by the mass M (or equivalently, the radius r_{200}), and the concentration paramater c.

Simulations show that the concentration index is strongly correlated with the mass and the redshift. Approximately

$$c \propto \frac{M^{-1/9}}{M_*}(1+z)^{-1}$$

where M_* is the charateristic halo mass at a given mass (similar to the Schechter L_* for the luminosity function of galaxies, and z is the redshift of the halo.

Hence low mass halos have higher concentration.

The figures below shows the fits to halos from simulations

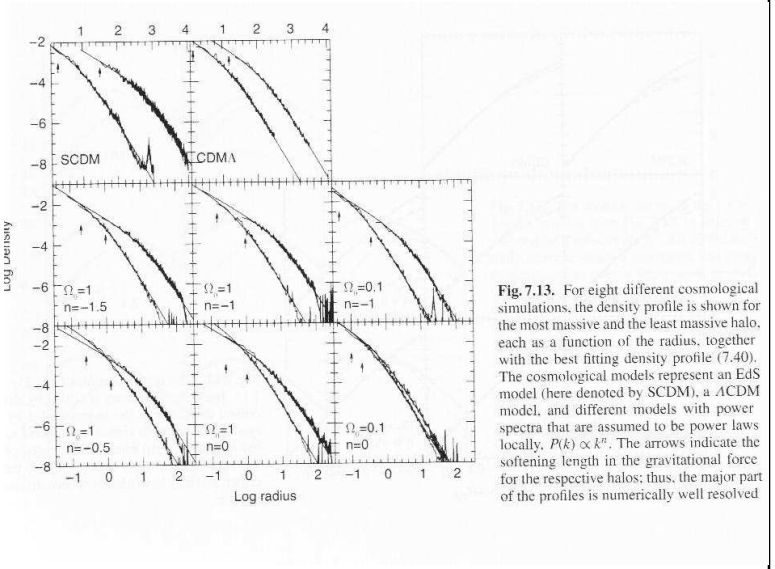

Fig. 7.13. For eight different cosmological simulations, the density profile is shown for the most massive and the least massive halo, each as a function of the radius, together with the best fitting density profile (7.40). The cosmological models represent an EdS model (here denoted by SCDM), a ΛCDM model, and different models with power spectra that are assumed to be power laws locally, $P(k) \propto k^n$. The arrows indicate the softening length in the gravitational force for the respective halos; thus, the major part of the profiles is numerically well resolved

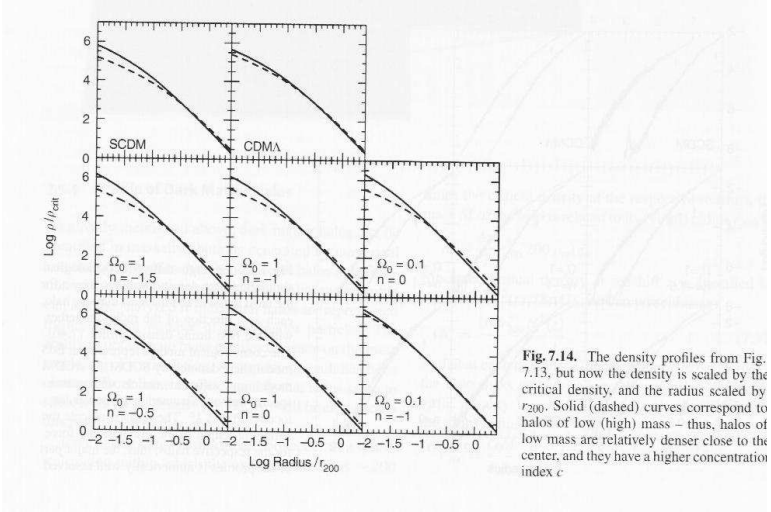

Fig. 7.14. The density profiles from Fig. 7.13, but now the density is scaled by the critical density, and the radius scaled by r_{200}. Solid (dashed) curves correspond to halos of low (high) mass – thus, halos of low mass are relatively denser close to the center, and they have a higher concentration index c

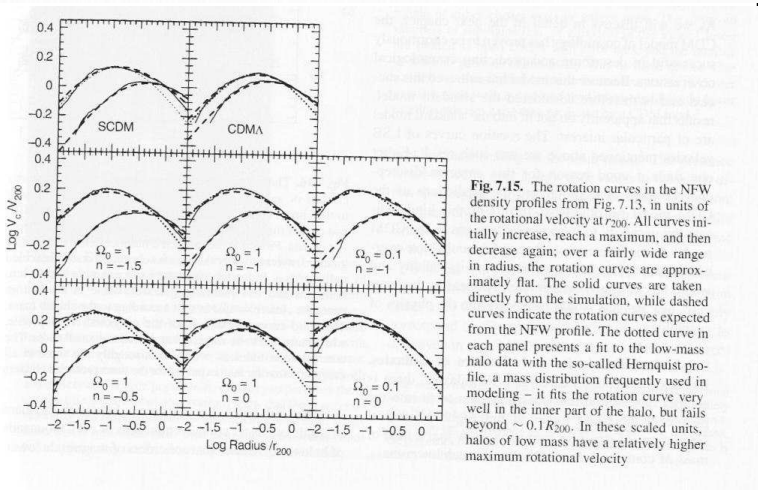

Fig. 7.15. The rotation curves in the NFW density profiles from Fig. 7.13, in units of the rotational velocity at r_{200}. All curves initially increase, reach a maximum, and then decrease again; over a fairly wide range in radius, the rotation curves are approximately flat. The solid curves are taken directly from the simulation, while dashed curves indicate the rotation curves expected from the NFW profile. The dotted curve in each panel presents a fit to the low-mass halo data with the so-called Hernquist profile, a mass distribution frequently used in modeling – it fits the rotation curve very well in the inner part of the halo, but fails beyond $\sim 0.1 R_{200}$. In these scaled units, halos of low mass have a relatively higher maximum rotational velocity

4.2 Comparison to observations

The easiest test to make, is to compare the density profiles of clusters to those of the simulations (the NFW profiles, and variants).

Below we show the comparison of mass profiles derived from X-ray data to those of NFW profiles:

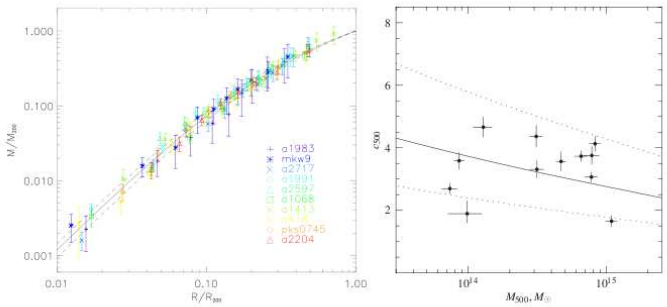

Figure 1: **Left:** Integrated mass profiles of 10 clusters in the temperature range 2 - 9 keV, observed with *XMM-Newton* (from Pointecouteau et al. 2005). For each cluster, the mass is scaled to M_{200} and the radius to R_{200}. The black line corresponds to the mean scaled best-fitting NFW model:, the dashed lines the associated standard deviation. **Right:** Concentration parameter vs mass relation for NFW model fits to the total density profiles of 12 clusters in the temperature range 0.7 - 9 keV, observed with *Chandra* (from Vikhlinin et al. 2006). The solid line shows the average concentration of CDM haloes from simulations; the dotted lines show the associated 2σ scatter.

It is remarkable how good the fit is, and the concentration index is well within the limits expected for the clusters.

Another (simpler) way to do this, is by looking at the distribution of the galaxies within the clusters. Again, a good fit is found:

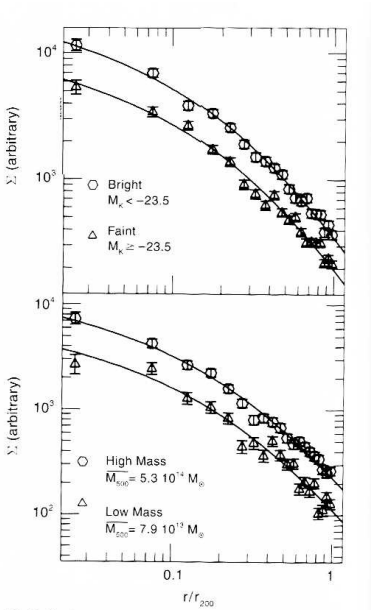

Fig. 7.16. The galaxy distribution averaged over 93 nearby clusters of galaxies, as a function of the projected distance to the cluster center. Galaxies have been selected in the NIR, and cluster masses, and thus r_{200}, have been determined from X-ray data. Plotted is the projected number density of cluster galaxies, averaged over the various clusters, versus the scaled radius r/r_{200}. In the top panel the galaxy sample is split into luminous and less luminous galaxies, while in the bottom panel the cluster sample is split according to the cluster mass. The solid curves show a fit of the projected NFW profile, which turns out to be an excellent description in all cases. The concentration index is, with $c \approx 3$, roughly the same in all cases, and smaller than expected for the mass profile of clusters

Halo Structure of galaxies

For galaxies, it is much harder to measure the dark matter halo structure. Gas velocity curves do not extend far enough. Just as an exercise, estimate the virial radius of a galaxy like our own Milky Way. Just assume that $V_{200} = 150 km/s$. For r_{200} we would derive $150/(10 * 70)$ Mpc $=$ 210 kpc, very much beyond the sizes of (gas) disks.

Hence we need different tracers to estimate the masses and mass profiles. Options are:

- 1. kinematics of satellite galaxies
- 2. kinematics of very distant stars
- 3. deflection of light

Below we show some examples.

1) Satellites. The SDSS project has measured a large number of velocities of galaxies. Some of these galaxies are close together on the sky, and sometimes, these galaxies are bound. Usually, a galaxy has only 1 satellite galaxy with a measured velocity. To still allow the measurement of a signal, we combine all the satellite galaxy-main galaxy pair. We restrict the main galaxies to those galaxies with similar luminosity.

By careful analysis, the velocity dispersion of the satellite system can be measured. Prada et al (2003) found this results:

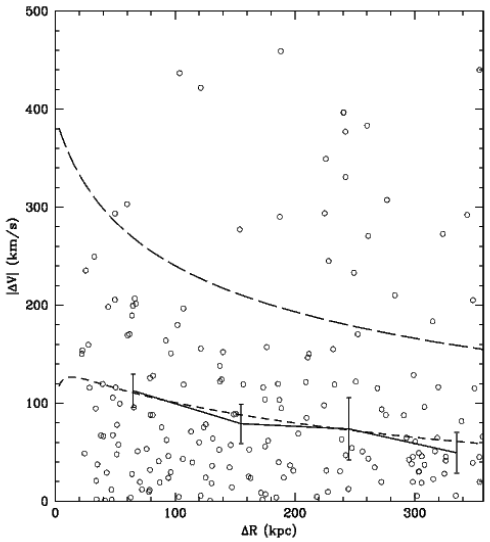

FIG. 9.—Same as in Fig. 7, but with the removal of the interlopers. The solid curve with the error bars shows the rms velocity after removal of interlopers. As in Fig. 8, the rms is clearly declining and consistent with the NFW profile (*short-dashed curve*) with $M_{\rm vir} = 1.5 \times 10^{12}\ M_\odot$. The long-dashed curve shows the escape velocity from the NFW halo of this mass. All satellites above the escape velocity curve are interlopers.

The results are very nicely described by an NFW profile.

2. Kinematics of very distant stars. This method is most easily applied to our own galaxy (but studies of external galaxies are coming !). A very recent example is shown below (Xue et al. 2008):

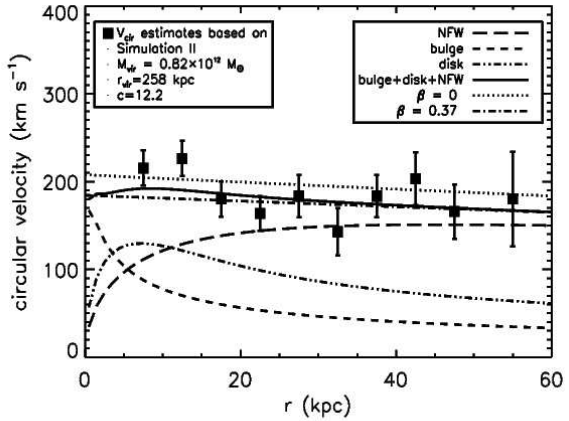

FIG. 16.—Circular curve estimates matched by a combination of a stellar bulge and disk and an unaltered NFW dark matter profile. The solid line indicates the best-fit circular velocity curve to the $V_{\rm cir}(r)$ estimates, while the large symbols represent the $V_{\rm cir}(r)$ estimates. The contributions of the adopted model components (i.e., disk, bulge, and halo) and the circular velocity curves based on the Jeans equation are plotted in different line styles. Estimates of virial mass, $M_{\rm vir}$, virial radius, $r_{\rm vir}$, and concentration parameter, c, are labeled on the plots.

The authors were able to measure the velocity dispersion to 60kpc. This is a record - but still much smaller than the virial radius r_{200} which is at the level of 200 kpc.

3. Gravitational deflection of light. This method relies on the bending of light through gravity. A beautiful example is when the galaxy produces an Einstein ring of a source behind it.

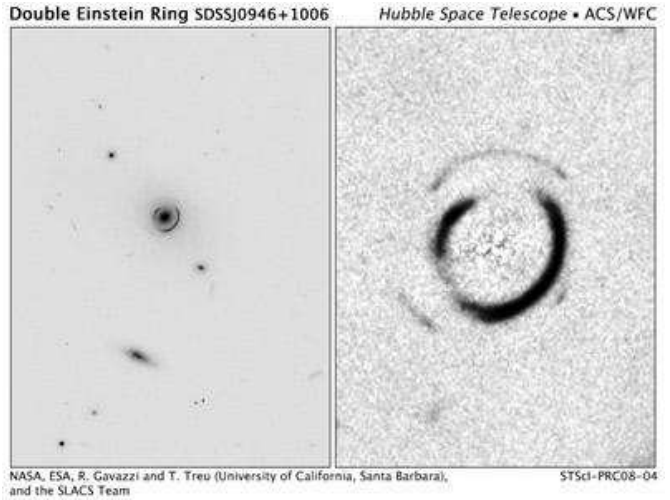

In this case, two galaxies are located nearly precisely behind another. The mass inside the ring is well determined. However, this method does not extend to very large radii - one would have to analyze the weaker deflections. This is possible, but much harder.

An example is shown below (van Uitert et al 2011, AA 534, 14). In this case, the shapes of many background galaxies are averaged together. The measured γ is the average elongation of background galaxies. This is mostly due to the weak gravitational lensing by the foreground galaxy. The measured signal can be compared to the theoretical expectation.

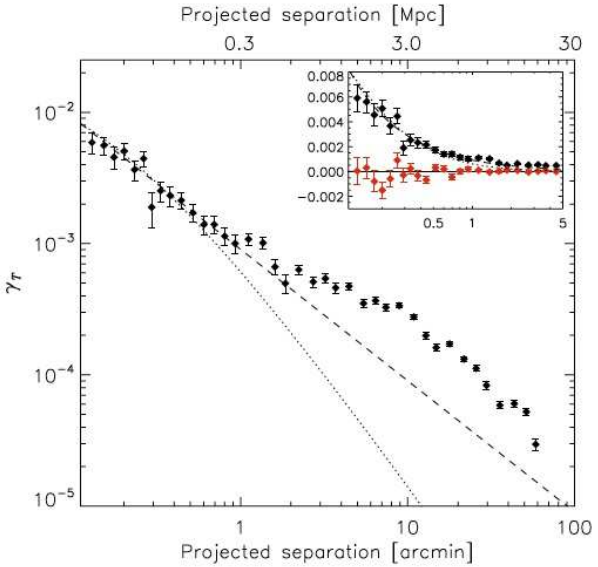

Fig. 5. Galaxy-mass cross-correlation function around 7.3×10^5 apparent magnitude selected lenses measured with 5.9×10^6 sources. The black symbols are the tangential shear, the red symbols are the cross shear. The top axis shows the projected separation in physical units for the median lens redshift $z_{\rm med} = 0.34$. The inset shows the signal on a linear scale for small separations. The signal has been corrected for contributions from systematic shear, and boosted to account for source galaxy contamination. The dashed (dotted) line shows the best fit SIS (NFW), fitted to the shear on scales between 0.2 and 0.6 arcmin. The clustering of galaxies causes excess shear at scales >1 arcmin.

Problems with dark matter halos and real galaxies

Generally, two problems exist: some galaxies may have rather large central cores (larger than expected in the NFW profiles), and the dark matter halos in the simulations have too many "sub-halos".

- Cores

Low surface brightness galaxies have rotation curves which rise slowly. This is unexpected for galaxies with NFW halos. Naray et al 2007 (arxiv: 0712.0860) show this result:

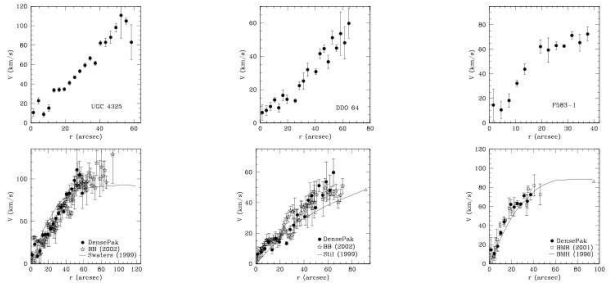

FIG. 1.— Additional observations of UGC 4325, DDO 64, and F583-1. *Top row:* Position of DensePak array on the Hα images of UGC 4325 and DDO 64 and the *R*-band image of F583-1. *Second row:* Observed DensePak velocity field with new pointings. Empty fibers are those without detections. *Third row:* Updated DensePak rotation curves. *Bottom row:* Updated DensePak rotation curves plotted with long-slit Hα and H I rotation curves. [*See the electronic edition of the Journal for a color version of this figure.*]

Fits with NFW profiles are hard. The rise of the rotation curve is too slow:

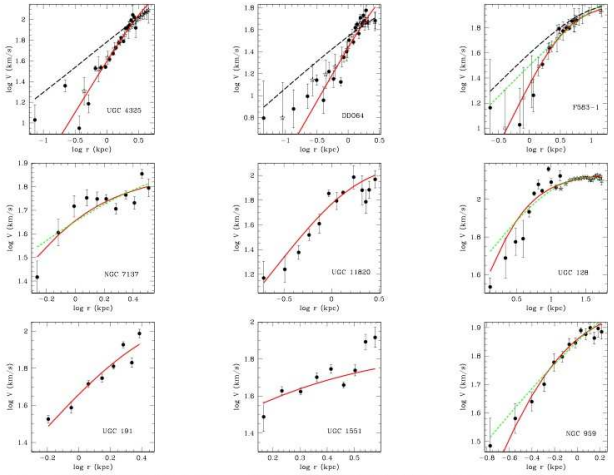

FIG. 4.— Halo fits to the DensePak rotation curves. The red solid line is the best-fit isothermal halo, the green short-dashed line is the best-fit unconstrained NFW halo, and the black long-dashed line is the best-fit NFW_{constr} halo. NFW_{constr} fits were only made to UGC 4325, DDO 64, and F583-1. [*See the electronic edition of the Journal for a color version of this figure.*]

However, it is possible that other processes play a role. For example, rotation may not dominate the gas kinematics.

- Substructure

The halos from simulations look smooth - but are not as smooth as might be. Many show subhalos. An example is : (e.g., Springel et al. 2008, arxiv 0809.0898)

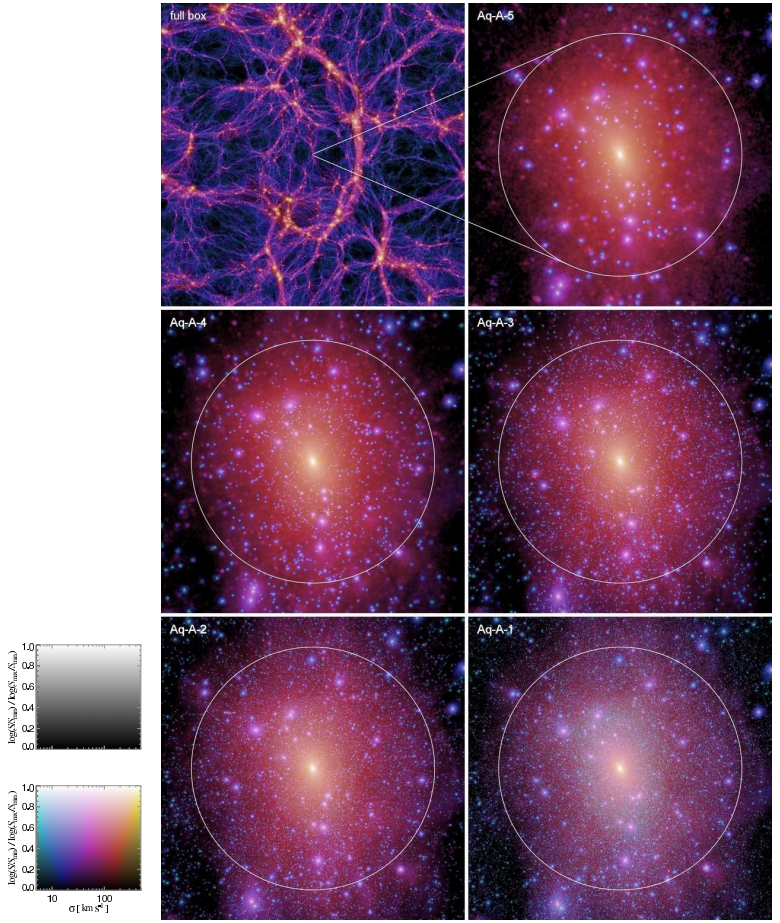

Figure 2. The top left panel shows the projected dark matter density at $z = 0$ in a slice of thickness 13.7 Mpc through the full box (137 Mpc on a side) of our 900^3 parent simulation, centred on the 'Aq-A' halo that was selected for resimulation. The other five panels show this halo resimulated at different numerical resolutions. In these panels, all particles within a cubic box of side-length $2.5 \times r_{50}$ centred on the halo are shown. The image brightness is proportional to the logarithm of the squared dark matter density $S(x, y)$ projected along the line-of-sight, and the colour hue encodes the local velocity dispersion weighted by the squared density along the line-of-sight. We use a two-dimensional colour table (as shown on the left) to show both of these quantities simultaneously. The colour hue information is orthogonal to the brightness information; when converted to black and white, only the density information remains, with a one-dimensional grey-scale colour map as shown on the left. The circles mark r_{50}.

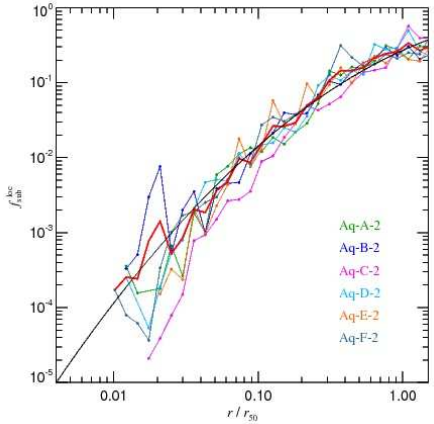
10^0
10^{-1}
10^{-2}
10^{-3}
10^{-4}
10^{-5}
$f_{\rm sub}^{\rm acc}$
0.01
0.10
1.00
r / r_{50}
Aq-A-2
Aq-B-2
Aq-C-2
Aq-D-2
Aq-E-2
Aq-F-2